

<https://doi.org/10.1038/s43246-024-00457-9>

Elastomers mechanically reinforced and toughened with CO₂ gas

Check for updates

Yohei Miwa^{1,2}✉, Hanako Yoneda¹, Takehito Ohya¹, Kazuma Okada¹, Rina Takahashi¹, Hayato Nakamura¹, Shoei Shimosaki¹, Kei Hashimoto¹ & Shoichi Kutsumizu¹

Gas-responsive polymers have recently attracted considerable interest as unconventional smart materials that provide a new path toward the utilization of specific gases including CO₂. Herein, we report gas-responsive elastomers that enhance mechanical properties, such as modulus, strength, stretchability, and toughness with CO₂ gas. Various types of amine groups are introduced into polydimethylsiloxane elastomers to achieve the gas-induced mechanical reinforcement. In these elastomers, the amines form ionic crosslinks with CO₂ gas that mechanically strengthen the materials. Furthermore, nanodomains formed via microphase separation of the ionic components behave similarly to viscoelastic nanofillers that dissipate a large amount of energy during deformation, thereby remarkably toughening the elastomers. Surprisingly, the fracture energy of the elastomer with diamine increases ~35 times in CO₂ gas compared with that in N₂ gas. Furthermore, the elastomers sensitively respond even to CO₂ gas concentrations as low as 10 % and are remarkably toughened. Our design concept is widely applicable to the CO₂ reinforcement of other polymers, such as polyethylene.

In nature, gases trigger vital stimuli in living organisms. Animals smell gases to find and distinguish foods, associates, and dangers. Not only animals but also insects and plants sense gases, such as CO₂. For example, some plants control stomatal conductance in their leaves depending on the CO₂ concentration¹. Mosquitos detect CO₂ gas in animals' breaths to identify targets². Similarly, synthetic materials that respond to specific gases and switch their properties have been developed^{3–6}. However, the applications of such gas-responsive materials have remained limited because they are mostly produced in the form of solutions^{7–13}, liquids^{14–17}, nanoparticles¹⁸, hydrogels^{19,20}, and organogels^{21,22}. From the viewpoint of applications, gas-responsive bulk materials that can be molded into sheets, membranes, plates, and objects of various shapes are strongly desired. However, the field of gas-responsive bulk materials is almost unexplored and considerably few polymeric^{23–26}, metallic²⁷, and ceramic²⁸ materials that can enhance their functions with the aid of specific gases have been reported. In particular, materials that respond to CO₂ gas are important because it is one of the major greenhouse gases and its reduction, capture, and effective utilization are imperative to prevent global warming. To date, various chemical materials such as membranes^{29,30}, nanoporous materials³¹, catalysts^{32,33}, and reactive monomers^{34,35} have been developed to capture, separate, and utilize CO₂ gas. In this report, CO₂-responsive bulk materials that switch their mechanical properties with CO₂ gas have been reported. Moreover, we propose gas-induced mechanical reinforcement to enhance the mechanical

properties (i.e., modulus, strength, stretchability, and toughness) of bulk materials using specific gases. The materials exhibit remarkable enhancements in mechanical properties upon exposure to even low concentrations of CO₂ and some other gases. Moreover, these materials offer broad application prospects, including but not limited to sensors, tunable adhesives, shape-memory materials, actuators, and strength-tunable materials. These materials will provide a new path toward the effective utilization of CO₂ gas.

Results and discussion

Material design

To achieve gas-induced mechanical reinforcement, we programmed components that generate reinforcement structures and/or morphologies through chemical and/or physical interactions with specific gases. In particular, the formation of physical or chemical crosslinks, the induction of microphase separations, and the transitions in morphologies were considered. The formation of crosslinks is the simplest method to enhance the modulus and strength of materials. Moreover, the induction of microphase separation may be effective for toughening materials through the formation of nanodomains. If nanodomains are rubbery at room temperature, they behave similarly to viscoelastic nanofillers that prevent the fracture of the material. In this case, the material's properties can be tuned by varying the size, number density, and viscoelasticity of nanodomains.

¹Department of Chemistry and Biomolecular Science, Faculty of Engineering, Gifu University, Yanagido, Gifu 501-1193, Japan. ²PRESTO, Japan Science and Technology Agency, Kawaguchi Center Building 4-1-8, Honcho, Kawaguchi, Saitama 332-0012, Japan. ✉e-mail: miwa.yohei.y6@f.gifu-u.ac.jp

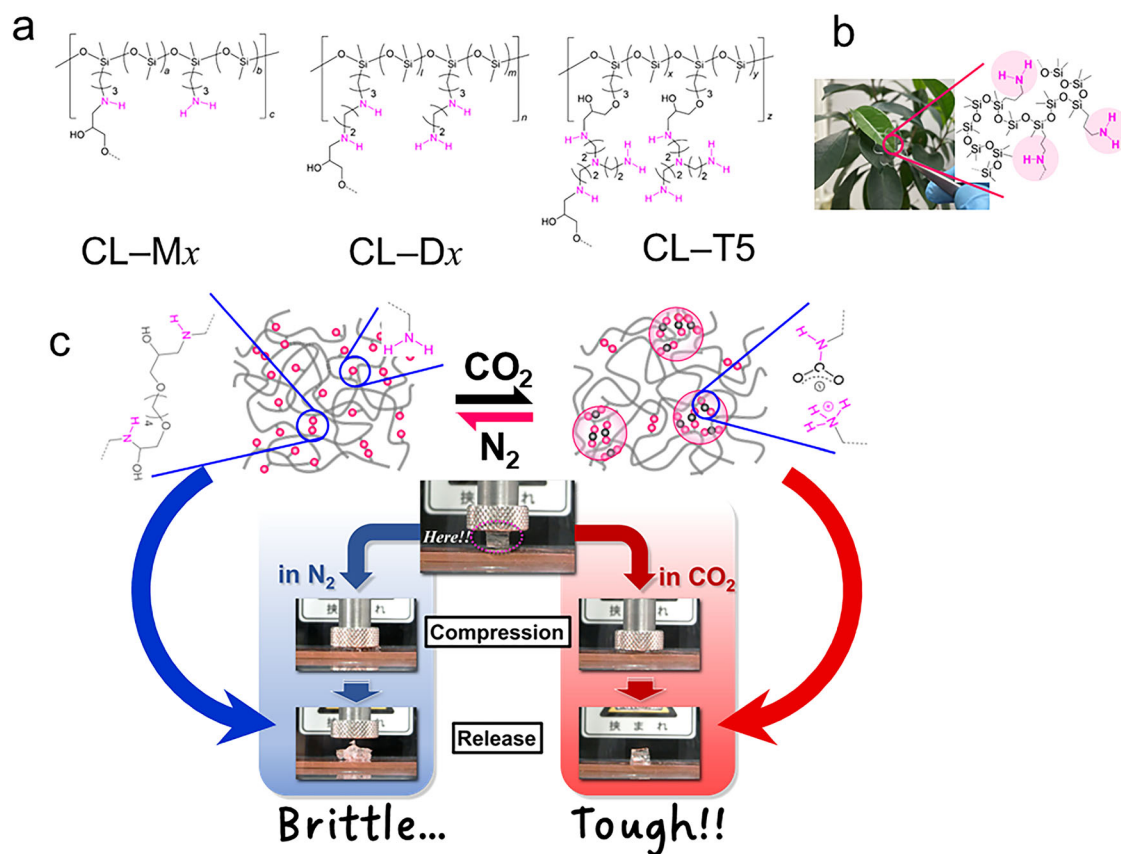


Fig. 1 | Molecular structures and CO₂ toughening behavior of elastomers.
a Chemical structures of PDMS elastomers modified with amines. **b** Photograph of a CL-M5 sheet that is colorless and transparent. **c** Compression behavior of a block of

CL-M5 in N₂ and CO₂ gases. CL-M5 is extremely toughened with CO₂ gas while it is brittle in a N₂ environment. See Supplementary Movie 3 and Supplementary Movie 4 in detail.

To demonstrate the aforementioned concept, we selected chemically crosslinked polydimethylsiloxane (PDMS) elastomers modified with amines (Fig. 1a). The high gas permeability of PDMS³⁶ facilitates a rapid reaction between gas molecules and amines even in the bulk material. Amines are converted to ammonium carbamates that function as ionic crosslinks upon a reaction with CO₂ gas¹⁶. Moreover, ammonium carbamates aggregate into nanodomains in the hydrophobic PDMS matrix (Fig. 1c). In this polymer, the size and viscoelasticity of the nanodomains can be tuned by varying the size of the amine moiety (Fig. 1a). The generated viscoelastic nanodomains effectively dissipate a large amount of energy and prevent crack propagation upon material deformation; thus, the fracture of the material is efficiently prevented (Fig. 1c).

Materials synthesis and characterization

PDMS samples having monoamine and diamine groups, denoted as PDMS-M_x and PDMS-D_x (*x* indicates the content of amine in mol%), respectively, were synthesized via ring-opening polymerization (Supplementary Fig. 1). PDMS-M_x and PDMS-D_x were characterized via ¹H-nuclear magnetic resonance (NMR) (Supplementary Fig. 2) and gel permeation chromatography (GPC). The weight-average molecular weight (*M_w*) and the polydispersity index (PDI) were determined via GPC using PDMS standards (Scientific Polymer Products Inc.); the amine concentrations determined via neutralization titration are listed in Table 1. PDMS-M_x and PDMS-D_x were chemically crosslinked using 1,4-butanediol diglycidyl ether (BDE; concentration = 8.5 × 10⁻⁵ mol g⁻¹). Crosslinked PDMS-M_x and PDMS-D_x were denoted as CL-M_x and CL-D_x, respectively (Fig. 1a). Additionally, CL-T5 wherein PDMS was modified using tris(2-aminoethyl)amine (TAEA) was obtained via the addition of TAEA to epoxy-modified PDMS (Fig. 1a). The *M_w* and PDI values of epoxy-modified PDMS (KF-1001, Shin-Etsu Chemical Co., Ltd.)

were determined to be 66700 and 1.89, respectively (Table 1). The concentration of the epoxy group was 2.9 × 10⁻⁴ mol g⁻¹. CL-T5 contained 3 wt% TAEA, i.e., the amine concentration in CL-T5 was 6.3 × 10⁻⁴ mol g⁻¹ (~4.7 mol%) without tertiary amine. The sheets of these elastomers (~1 mm thick) were colorless and transparent (Fig. 1b).

Microphase separation with CO₂ gas

CL-M5, CL-D9, and CL-T5 sheets rapidly trap CO₂ gas molecules even though they are relatively thick (~1 mm). The increase in the sheet weight under CO₂ gas flow was monitored at 25 °C (Fig. 2a). The trapped CO₂ molecules were slowly released under N₂ gas flow. The amounts of CO₂ molecules trapped in CL-M5, CL-D9, and CL-T5 were calculated to be 3.3 × 10⁻⁴, 5.1 × 10⁻⁴, and 2.1 × 10⁻⁴ mol g⁻¹, respectively. These values were nearly half of the values of the concentration of the amine groups in each sample, indicating the formation of ammonium carbamates (Fig. 2a)¹⁶. When our elastomer materials were heated, the trapped CO₂ was rapidly released (Supplementary Fig. 3). This result implies that the effect of CO₂ on our materials is easily canceled by heating the materials. The formation of ammonium carbamates was further verified via Fourier-transform infrared (FT-IR) spectroscopy bands, N-H bending, C=O stretching, and C-N stretching bands at 1580, 1640, and 1470 cm⁻¹, respectively¹⁶ (Fig. 2b). The formation of ammonium carbamates occurs even at low concentrations of CO₂ gas (Fig. 2c). For example, 72% of amines in CL-D9 were converted to ammonium carbamates even with the N₂/CO₂ (95/5) mixed gas. Hydrophilic ammonium carbamates aggregate into nanodomains in the hydrophobic PDMS matrix as illustrated in Fig. 1c. In the small-angle X-ray scattering (SAXS) patterns, a broad and relatively strong scattering peak is exhibited for the samples reacted with CO₂ gas owing to the formation of nanodomains, whereas marginal scattering from heterogeneities in the crosslinked PDMS matrix is observed in air (Fig. 2d). In case of

noncrosslinked PDMS–M5 and PDMS–D9, similar scattering from the nanodomains with CO₂ gas is observed; however, no scattering peak is detected in air (Supplementary Fig. 4). The size and number density of the nanodomains with ammonium carbamates were determined by simulating the experimental SAXS patterns. We found that the Yarusso–Cooper model³⁷ satisfactorily reproduces the experimental SAXS patterns (Fig. 2d). This model assumes that spherical nanodomains with a radius (R_1) are randomly distributed with the closest approach limitation ($2R_{ca}$) in the matrix. The sample volume occupied by one nanodomain is V_p . The

parameters used in the simulation of each sample are listed in Table 1. The volume ($V = \frac{4}{3}\pi R_1^3$, nm³) and number density (ND ((10 nm)⁻³) of nanodomains calculated using the simulation parameters are indicated in Fig. 2d. V increases with the increasing size of the amine group. Even though the V value of CL–M5 is relatively small, CL–M5 exhibits a considerably larger ND value than CL–D9, wherein the concentration of diamine side groups (~4.6 mol%) is comparable with the monoamine concentration in CL–M5. As shown in Fig. 2d, the intensity of the scattering peak of CL–M5 is small compared with that of CL–D9 despite the larger ND value of CL–M5, indicating that the electron density of the nanodomains in CL–M5 decreases upon the inclusion of polymer segments into the nanodomains. The inclusion of polymer segments into ionic aggregates is frequently observed in ionomers³⁸. In our study, nanodomains are efficiently formed even at low concentrations of CO₂ gas (N₂/CO₂ (90/10)) (Supplementary Fig. 5). Interestingly, V is almost insensitive to the CO₂ concentration, whereas ND increases with the increasing CO₂ concentration. This result confirms that the size of the amine group dominates the size and number density of the nanodomains upon CO₂ gas exposure.

Table 1 | Molecular characteristics of samples and parameters used for the simulation of SAXS patterns for samples with CO₂ gas

Notation	M_w^a	PDI ^a	Amine ^a (mol g ⁻¹)	Amine ^a (mol%)	R_1 (nm)	R_{ca} (nm)	V_p (nm ³)
CL–M5	61,200	1.81	6.8×10^{-4}	5.2	1.08	1.28	30.1
CL–M10	98,200	2.14	1.3×10^{-3}	10	1.01	1.17	21.1
CL–D5	43,000	1.59	6.2×10^{-4}	4.7	1.28	1.89	109
CL–D9	68,200	2.62	1.1×10^{-3}	9.2	1.22	1.83	73.1
CL–T5	66,700	1.89	6.3×10^{-4b}	4.7 ^b	1.24	2.09	85.0

^aValues for precursor polymers.

^bTertiary amine is not included.

Enhancement of viscoelastic properties using CO₂ gas

Upon the formation of nanodomains using CO₂ gas, additional relaxation occurs owing to molecular motions in the nanodomains in linear viscoelastic measurements (Fig. 3a–e). For CL–M5 (Fig. 3a) and CL–D9 (Fig. 3d), additional relaxation occurred even in the N₂/CO₂ (90/10)

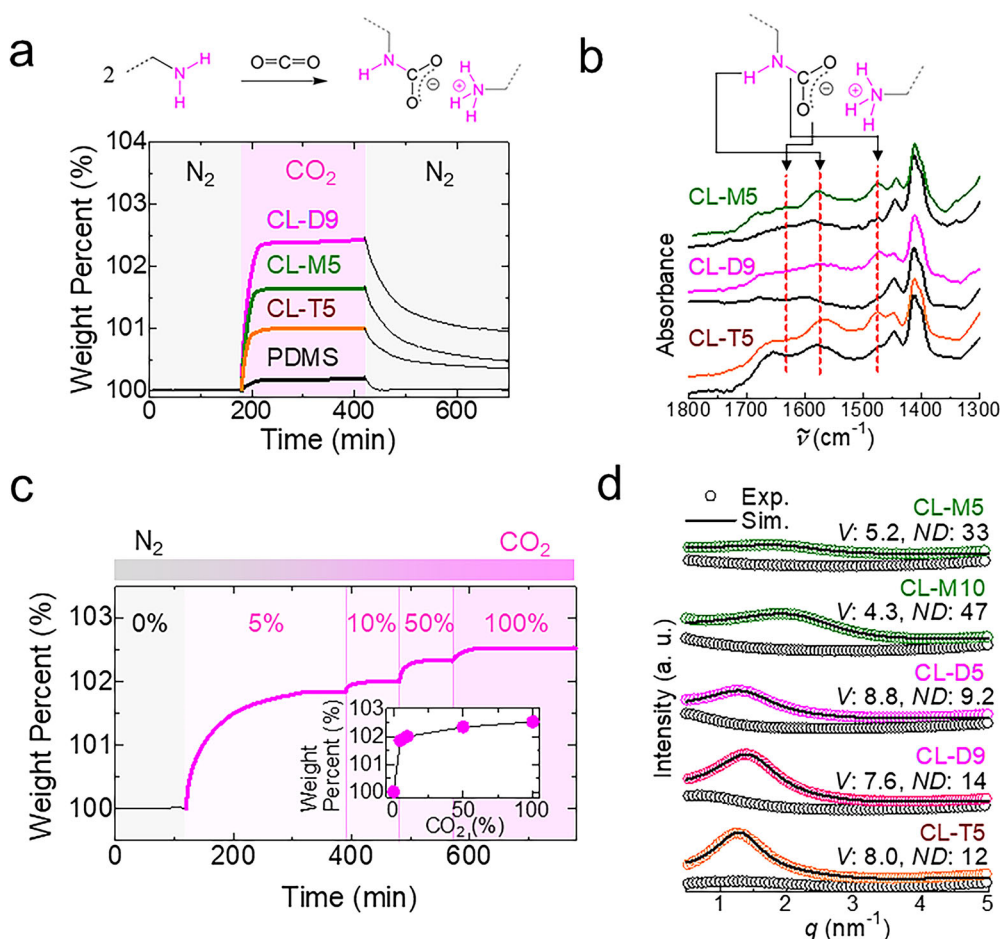


Fig. 2 | Effects of CO₂ on elastomer structure. **a** Weight changes of samples with different gas flows. The weights of samples increase with CO₂ gas. PDMS is a homopolymer without amines (KF-96H-50000CS, Shin-Etsu Chemical). The chemical reaction between primary amines and CO₂ is also shown. **b** FT-IR spectra of elastomers in N₂ (black) and CO₂ (colored) gases. Ammonium carbamates are generated with CO₂. **c** Weight changes of CL–D9 in N₂/CO₂ mixed gases with

different CO₂ concentrations. **d** Experimental and simulated SAXS patterns of elastomers. The SAXS patterns with and without CO₂ are indicated by the colored and black plots, respectively. The Yarusso–Cooper model is used for the simulation³⁷. V (nm³) and ND ((10 nm)⁻³) correspond to the volume and number density of nanodomains, respectively.

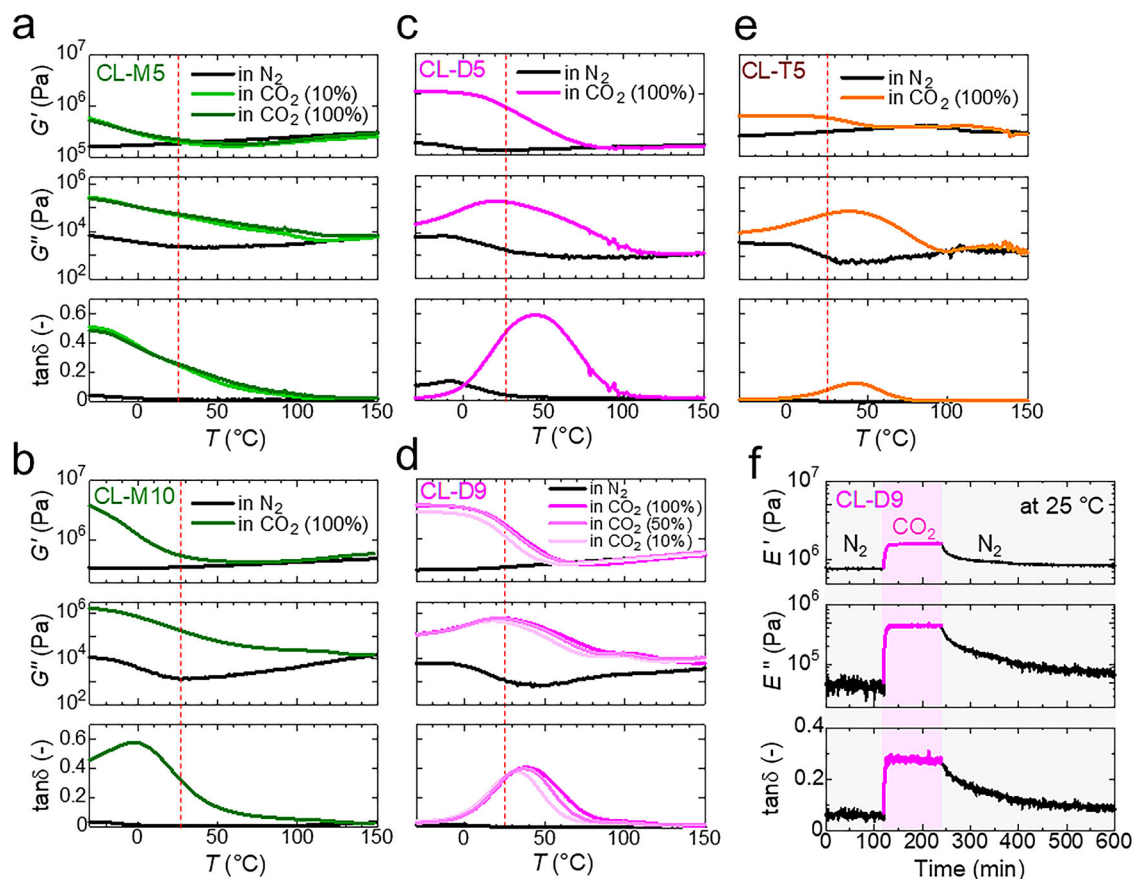


Fig. 3 | Effects of CO₂ on the viscoelastic properties of elastomers. Effects of each gas on the shear storage modulus (G'), shear loss modulus (G'') and loss tangent ($\tan\delta$) of 1 Hz for CL-M5 **a**, CL-M10 **b**, CL-D5 **c**, CL-D9 **d**, and CL-T5 **e** at 1 Hz.

For CL-M5 and CL-D9, N₂/CO₂ mixed gases were also used. The vertical broken line indicates 25 °C. **f** Changes in the tensile storage modulus (E'), tensile loss modulus (E''), and $\tan\delta$ of CL-D9 in N₂ and CO₂ gases measured at 1 Hz and 25 °C.

mixed gas. Because of this additional relaxation, the shear storage modulus (G'), shear loss modulus (G''), and loss tangent ($\tan\delta$, $G'' G'^{-1}$) of the elastomers increase considerably at room temperature. In particular, this effect is pronounced for CL-D5 (Fig. 3c) and CL-D9 (Fig. 3d) in which additional relaxations occur near room temperature. The relaxation temperatures determined from the G'' peaks of CL-M5, CL-M10, CL-D5, CL-D9, and CL-T5 are less than -30 °C, approximately -30 °C, 21 °C, 23 °C, and 39 °C, respectively, while the glass transition temperature (T_g) of PDMS measured using differential scanning calorimetry is ~ 122 °C (Supplementary Fig. 6). The relaxation temperature of the nanodomains increases with the increasing size of amine group, signifying that the viscoelastic properties of our materials can be tuned by modifying the size and content of the amine group upon CO₂ gas exposure. Among our materials, CL-D9 toughened with CO₂ gas exhibits the largest G'' value at room temperature (25 °C) (Fig. 3d). Mullins reported that G' and the fracture energy values of elastomers are correlated³⁹. This study demonstrates that effective energy dissipation during deformation is crucial for toughening materials. In fact, CL-D9 with CO₂ gas exhibited high toughness as discussed below. Furthermore, CO₂ gas rapidly changed the viscoelasticity of our materials owing to the high gas permeability of PDMS. The tensile storage modulus (E'), tensile loss modulus (E''), and loss tangent ($\tan\delta$, $E'' E'^{-1}$) of CL-D9 instantaneously increase with CO₂ gas flow, whereas these parameters gradually return to their initial values when exposed to N₂ gas flow at 25 °C (Fig. 3f). This behavior is consistent with the results of the CO₂ uptake shown in Fig. 2a. The increases in G' and G'' with the increasing CO₂ concentration were similarly observed for PDMS oils containing amine groups¹⁶. However, the values of G' and G'' were less than one kPa because of their small molecular weight and the absence of the chemical crosslinks.

Enhancement of mechanical properties via reinforced with gases

Our elastomers are considerably toughened with CO₂ gas owing to the formation of viscoelastic nanodomains. For example, a CL-D9 sheet could be very easily stabbed in air (Supplementary Movie 1). However, this sheet became remarkably toughened with CO₂ gas (Supplementary Movie 2). To quantitatively estimate the toughness of the materials, fracture energies were measured via tearing tests using trouser-shaped test pieces⁴⁰ (Fig. 4a). The fracture energies of the elastomers are dramatically enhanced when exposed to CO₂ gas. Our elastomers exhibit considerable brittleness in N₂ gas and in air, where their fracture energy values remained less than 60 J m^{-2} . However, the fracture energies of elastomers considerably increase with CO₂ gas (Fig. 4a). In particular, CL-D9 in CO₂ gas (100%) exhibits a maximum value of $\sim 1420 \text{ J m}^{-2}$. This value is ~ 35 times as large as that measured in N₂ gas. Furthermore, our materials are effectively toughened even at low concentrations of CO₂ (Fig. 4a). For example, the fracture energy value of CL-D9 in the case of the N₂/CO₂ (90/10) mixed gas is $\sim 970 \text{ J m}^{-2}$, which is ~ 25 times that of CL-D9 in N₂ gas. Although the effect of CO₂ gas concentration is examined only for CL-M5 and CL-D9 in this study, a similar trend is expected for the other samples. Not only CO₂ gas, but also other gases such as hydrogen chloride (HCl) and acetic anhydride (AcAh) gases are available for toughening our elastomers (Fig. 4a). Such HCl and AcAh gases form ammonium chloride and amide groups in our elastomers, respectively (Supplementary Fig. 7a). Such groups aggregate into nanodomains, functioning as viscoelastic nanofillers (Supplementary Fig. 7b and Supplementary Fig. 7c). Unlike ammonium carbamates, these groups are stable at room temperature in air.

The toughening behavior of the presented elastomers is affected by the changes in their viscoelasticity with the increasing concentrations of CO₂ gas. Mullins demonstrated that the fracture energy value of elastomers

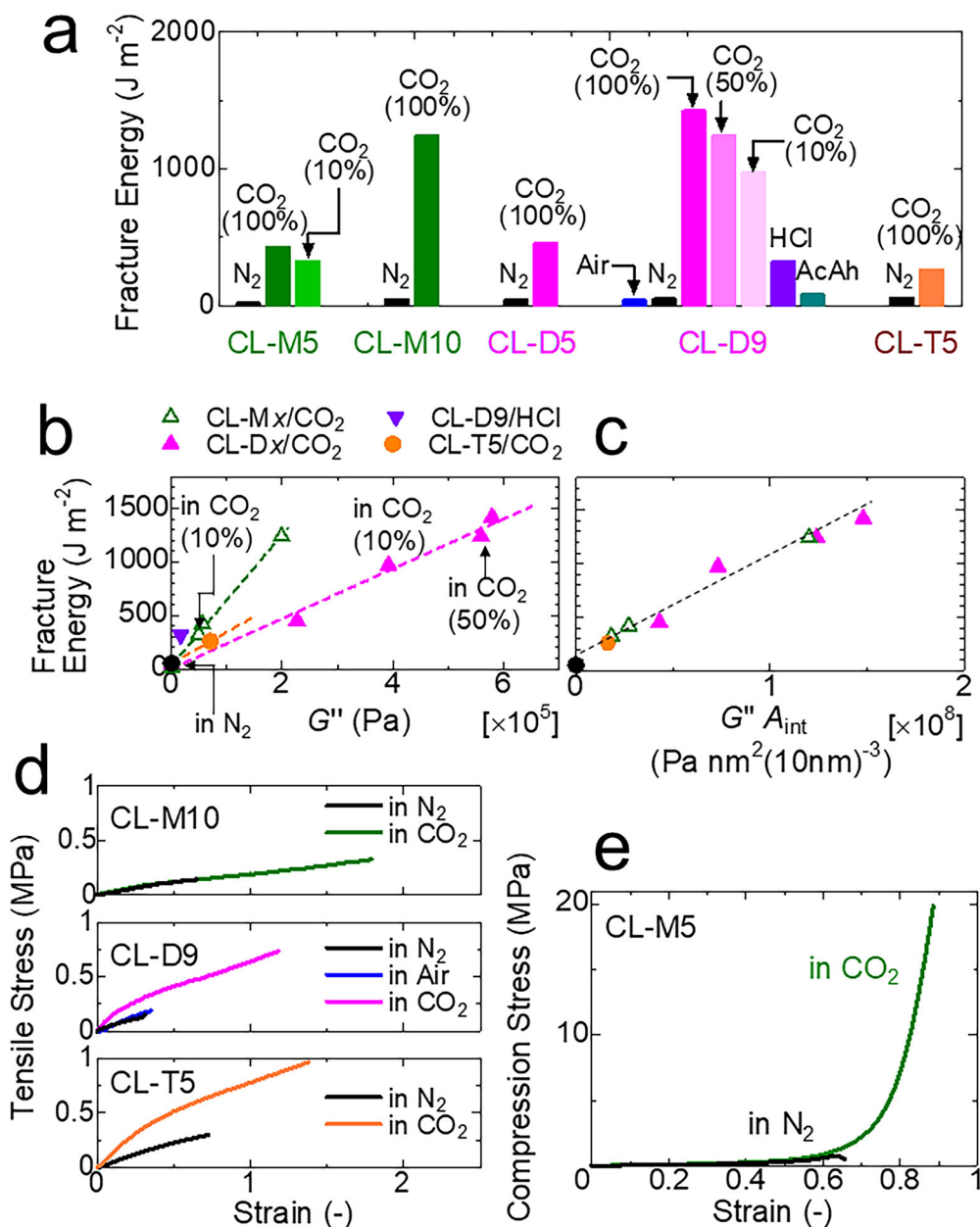


Fig. 4 | Effects of CO₂ on the mechanical properties of elastomers. **a** Effects of different gases on the fracture energies of elastomers. For CL-M5 and CL-D9, N₂/CO₂ mixed gases were also used. Fracture energies were determined by tearing tests for trouser-shaped test pieces⁴⁰. **b** Relationship between the fracture energy and

shear loss modulus (G'') of elastomers at 25 °C. **c** Fracture energy against $G''A_{int}$ ($A_{int} = 4\pi R_1^2 \times ND$). **d** Tensile testing of elastomers measured at 26 °C ± 1 °C in N₂, air, and CO₂ gases. The strain rate was 0.09 s⁻¹. **e** Compression tests for CL-M5 measured at 26 °C ± 1 °C in N₂ and CO₂ gases. The strain rate was 0.03 s⁻¹.

exhibits a correlation with their G'' ³⁹. Similarly, the fracture energy values of the elastomers in our study exhibits a correlation with G'' (Fig. 4b), whereas they do not exhibit a correlation with G' and $\tan\delta$ (Supplementary Fig. 8). This result clearly indicates that the generation of viscoelastic nanodomains⁴¹ is the main cause for the toughening of our materials. We speculate that the fracture of our materials is prevented owing to energy dissipation via the viscoelastic behavior of the nanodomains. Furthermore, each elastomer exhibits different fracture-energy-versus- G'' relations. CL-Mx (green) and CL-Dx (pink) exhibit different slopes, while CL-Dx and CL-T5 (orange) show similar fracture-energy-versus- G'' relations. Moreover, the relation of CL-D9 with HCl deviates from the relation of CL-Dx with CO₂ gas. Although the viscoelasticity of nanodomains mainly dominates the elastomer toughness, the morphology (size and ND) of nanodomains is also expected to affect the elastomer toughness. Figure 4c shows that the fracture energy values of all elastomers exhibit a single

relation in terms of a value of $G'' \times A_{int}$ where A_{int} represents the total area of the interface between the nanodomains and matrix for a constant sample volume of 1000 nm³, which is calculated using $4\pi R_1^2 ND$ (nm²(10 nm)⁻³). This result demonstrates that the nanodomain interface plays an important role in the toughening of our elastomers in addition to the viscoelasticity of nanodomains. At the present stage, we speculate that the interface of nanodomains prevents the propagation of microcracks in the material, thereby functioning as a toughening mechanism.

Contrary to the poor stretchability and fracture stress in N₂ gas, the modulus, stretchability, and fracture stress of our elastomers drastically increases with the increasing CO₂ concentration owing to the formation of nanodomains that function as physical crosslinks (Fig. 4d). In case of CL-Mx samples, nanodomains are soft and do not function as effective physical crosslinks at room temperature because the relaxation temperature of nanodomains is considerably lower than room temperature (Fig. 3a, b).

Therefore, the modulus of CL–M10 is not remarkably enhanced with CO₂ gas while the stretchability is largely improved owing to the prevention of fracture. The toughening of our elastomers with CO₂ gas is displayed during the compression tests. Upon compression, a block of CL–M5 is completely fractured in N₂ gas (Fig. 4e, Supplementary Movie 3). However, a CL–M5 block reacted with CO₂ gas does not fracture even at high compression (~20 MPa) despite the generation of some cracks (Fig. 4e, Supplementary Movie 4).

Role of detachment of ammonium carbamates from nanodomains in elastomer toughening

To understand the effects of nanodomains on material toughening, in situ SAXS measurements were conducted for CL–D9 under stretching. In this experiment, the specimen was stretched in the horizontal direction at a strain rate of 0.09 s⁻¹, and two-dimensional (2D) SAXS patterns were recorded at an exposure time of 1 s. One-dimensional (1D) SAXS patterns were extracted from the stretching and transverse directions with a narrow angle range ($\pm 5^\circ$) in the 2D SAXS pattern (Fig. 5a). The structural information of the nanodomains for each direction was separately obtained from the simulations of the 1D SAXS patterns based on the Yarusso–Cooper model³⁷ (Fig. 5b). In Fig. 5c, the R_1 , V , and ND values of the nanodomains were plotted as a function of strain for each direction. Interestingly, the thickness of nanodomains along the stretching direction slightly decreases upon stretching, as illustrated in Fig. 5d. This is attributed to the detachment of strongly stretched ammonium carbamates from the nanodomains. Moreover, the V value of nanodomains gradually decreases with stretching (Fig. 5c). Herein, oblate spheroid-shaped nanodomains with a short axis along the stretching direction are assumed to calculate V . The size and distribution of the oblate spheroid-shaped nanodomains along the transverse direction do not substantially change with stretching because the stacking of ammonium carbamates is rearranged along the transverse direction with stretching to reduce the steric constraint of stretched polymer chains attached to ammonium carbamates (Fig. 5d); this indicates that the stress is

concentrated at the nanodomains, which promotes mechanical reinforcement. Furthermore, the detachment of strongly stretched ammonium carbamates from nanodomains plays an important role in dissipating the excess stress locally concentrated in the stretched material, thereby preventing the fracture of our material under high stretching⁴². A similar toughening mechanism for covalently cross-linked networks via detachment of coexistent weak crosslinks such as the ionic one has been frequently observed⁴³.

Toughening of polyethylene with CO₂ gas

To demonstrate the applicability of our method to other polymers, the mechanical reinforcement of polyethylene (PE) with CO₂ gas was examined. PE is one of the most important polymers in our modern society. Vast amounts of PE are used daily as films, sheets, plates, tubes, and moldings. Therefore, the mechanical reinforcement of PE with specific gases can exemplify the remarkable impact our findings on potential applications and technologies. In this study, we prepared a TAEA-modified PE film (E–T), as shown in Fig. 6a, with a thickness of ~200 μm . E–T rapidly traps CO₂ gas molecules via the formation of ammonium carbamates (Supplementary Fig. 9a and Supplementary Fig. 9b). The trapped CO₂ is quickly released when the specimen is heated (Supplementary Fig. 9c). The generated ammonium carbamates microphase-separate into nanodomains in the PE matrix (Fig. 6b). The V and ND values of nanodomains determined via the Yarusso–Cooper model simulation³⁵ of the SAXS pattern are 3.4 (nm³) and 22 ((10 nm)⁻³), respectively. The formation of nanodomains with CO₂ gas mechanically reinforces and toughens E–T. The E' and E'' of E–T increase more than twofold with CO₂ gas (Fig. 6c). Owing to the mechanical reinforcement with CO₂ gas, the fracture stress of E–T in CO₂ gas (~14 MPa) is much higher than that in N₂ (~10 MPa) during the tensile test (Fig. 6d). The fracture energy of E–T increases from 3500 J m⁻² in N₂ to 4800 J m⁻² in CO₂ gas (Supplementary Fig. 9d). E–T is also reactive with HCl, AcAh, and acetic acid (AcOH) gases (Supplementary Fig. 10). Although AcOH molecules are released from E–T upon heating, E–T/HCl and E–T/AcAh are stable even at 110 °C.

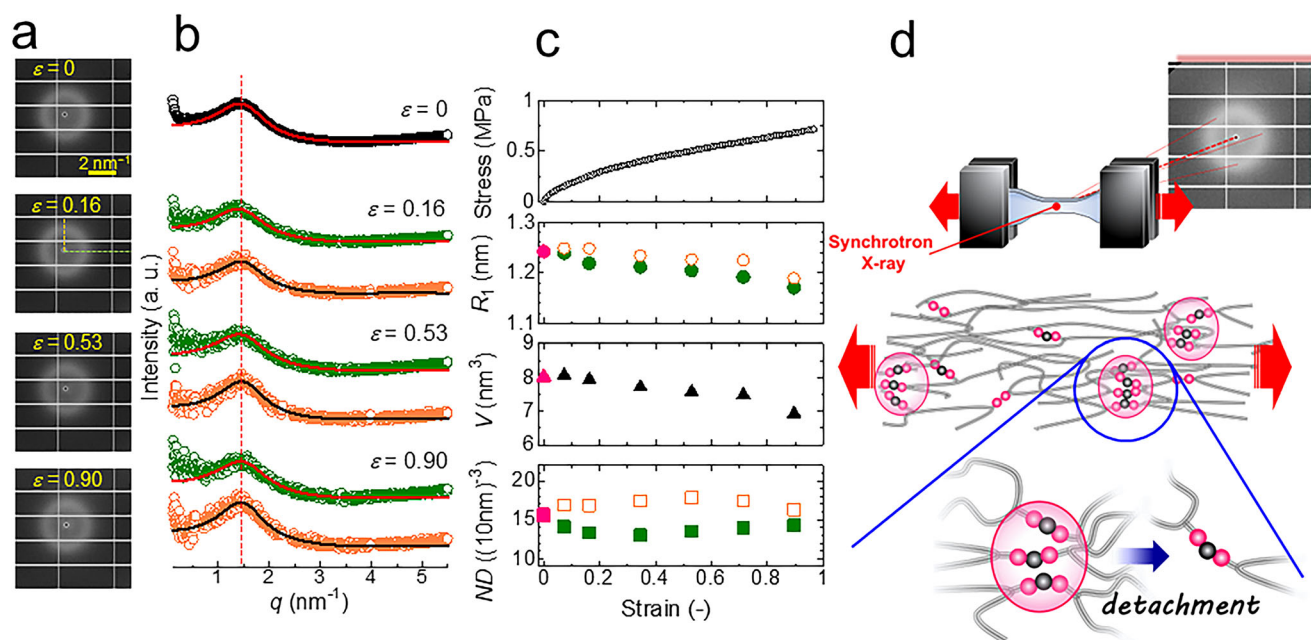


Fig. 5 | In situ SAXS analysis of CL–D9 with stretching. **a** 2D SAXS patterns of CL–D9 in CO₂ gas at various nominal strains (ϵ). The specimen was stretched at 0.09 s⁻¹ and 25 °C. **b** 1D SAXS profiles extracted from the stretching (green) and transverse (orange) directions ($\pm 5^\circ$). The experimental patterns were simulated using Yarusso–Cooper model³⁷. **c** Nominal stress, R_1 , V , and ND of CL–D9 in CO₂

gas against ϵ . Data for the unstretched state are indicated using the magenta symbols. For R_1 and ND , the data for the stretching and transverse directions are indicated using solid and open symbols, respectively. **d** Schematic illustration for the detachment of ammonium carbamate attached to highly stretched polymer chains from nanodomains.

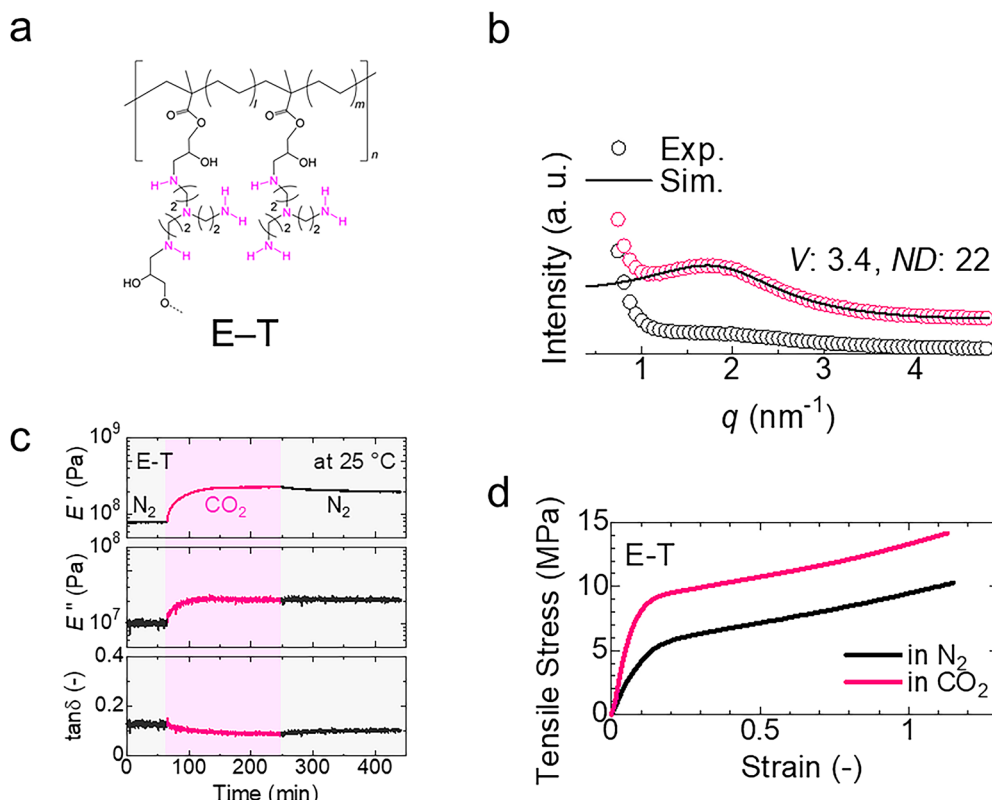


Fig. 6 | Mechanical reinforcement of polyethylene with CO₂ gas. **a** Chemical structure of E-T. **b** Experimental and simulated SAXS patterns of E-T. SAXS patterns with and without CO₂ are shown as magenta and black plots, respectively. The

Yarusso–Cooper model was used for the simulations³⁷. **c** Effects of CO₂ gas on E' , E'' , and $\tan\delta$ of E-T measured at 1 Hz and 25 °C. **d** Tensile behaviors of E-T measured at 26 °C ± 1 °C in N₂ and CO₂ gases. The strain rate was 0.09 s⁻¹.

Conclusion

Herein, we developed PDMS elastomers that are mechanically reinforced and toughened with CO₂, HCl, and AcAh gases. The key aspect of the material design involves programming chemical groups to form physical crosslinks with specific gases. Amine groups were examined as the simplest example of CO₂-responsive chemical groups. The amines form ammonium carbamates with CO₂ gas that physically crosslink polymer chains and mechanically reinforce the PDMS elastomers. Further, nanodomains with ammonium carbamates that function as viscoelastic nanofillers dissipate a large amount of energy upon material deformation and thus lead to mechanical toughening. Furthermore, this design can be applied to various polymers, such as PE. These CO₂-responsive materials exhibit considerable potential for practical applications, including but not limited to sensors, tunable adhesives, shape-memory materials, actuators, and strength-tunable materials. These materials provide a new path toward the effective utilization of CO₂ gas.

Methods

Details of sample preparation are described in the Supplementary Information.

Preparation of CL-Mx, CL-Dx, and CL-T5

CL-Mx and CL-Dx were prepared via the crosslinking of PDMS-Mx and PDMS-Dx with 1,4-butanediol diglycidyl ether (BDE; concentration = 8.5 × 10⁻⁵ mol g⁻¹). The M_w and PDI values of PDMS-Mx and PDMS-Dx are presented in Table 1. The amine concentrations of PDMS-M5, PDMS-M10, PDMS-D5, and PDMS-D9 were 5.2 mol% (6.8 × 10⁻⁴ mol g⁻¹), 10 mol% (1.3 × 10⁻³ mol g⁻¹), 4.7 mol% (6.2 × 10⁻⁴ mol g⁻¹), and 9.2 mol% (1.1 × 10⁻³ mol g⁻¹), respectively. Each polymer (7.94 g) was dissolved in dry THF (10 mL) with BDE (0.138 g) and poured into a Teflon petri dish. The mixture with PDMS-Mx was dried at 50 °C for 17 h. The obtained CL-Mx sheet was further dried at 90 °C for 48 h in a

vacuum. In the case of the mixture with PDMS-Dx, the mixture was dried at 35 °C for 39 h and then at 60 °C for 7 h. The mixture was further heated at 90 °C for 14 h in a vacuum to obtain a CL-Dx sheet. CL-T5 was obtained via the addition of tris(2-aminoethyl)amine (TAEA) to epoxy-modified PDMS (KF-1001, Shin-Etsu Chemical Co., Ltd.). The M_w and PDI values of KF-1001 were 66700 and 1.89, respectively. KF-1001 (9.70 g) and TAEA (0.300 g) were dissolved in dry chloroform (80 mL), and the solution was stirred at 90 °C for 4 h and poured into a Teflon petri dish. The solution was dried at 60 °C for 48 h, and the obtained CL-T5 sheet was further dried at 90 °C for 24 h in a vacuum. The thicknesses of the CL-Mx, CL-Dx, and CL-T5 sheets were ~1 mm.

Reaction of CL-D9 with HCl and AcAh gases

CL-D9 sheets and a glass petri dish containing HCl aqueous solution (35%) or AcAh were placed in a glass container. The glass container was kept at 40 °C for 24 h. The reacted sheets were vacuum dried at 35 °C for 24 h.

Preparations of E-T

Poly(ethylene-co-glycidyl methacrylate) (PEGMA, Sigma-Aldrich Co. LLC, 0.790 g) and TAEA (0.0605 g) were dissolved in dry toluene (30 mL) at 91 °C, and the solution was stirred for 5 h. The solution was then poured into a Teflon petri dish and slowly dried at 103 °C for 24 h. The obtained E-T film with a thickness of ~0.2 mm was further dried at 100 °C for 24 h in a vacuum. The obtained E-T film was transparent.

Measurements

Before the measurements, the sample sheets were further vacuum-dried at room temperature for at least 24 h and carefully placed into the instruments to avoid moisture absorption.

A 400 MHz JEOL-ECS400 spectrometer was used for ¹H-NMR measurements. CDCl₃ containing tetramethylsilane was used as a solvent. GPC

measurements were conducted using an EXTREMA HPLC system (JASCO Co.) equipped with a polystyrene gel column (Shodex GPC LF-804). THF was used as the eluent at 40 °C. PDMS standards (Scientific Polymer Products Inc.) were used for calibration.

DSC performed using a DSC7020 instrument (SII). The samples were heated from −150 °C to 100 °C at a rate of 10 °C min^{−1}. Thermogravimetry measurements were performed using STA200 (HITACHI) at a gas flow of 100 mL min^{−1}. N₂, CO₂, and N₂/CO₂ mixed gases were used. The concentration of the N₂/CO₂ mixed gas was controlled using a gas mixer CUBE GM3 (FCO Co., Ltd.).

An FT/IR-6600 spectrometer (JASCO Co.) equipped with a triglycine sulfate detector was used for FT-IR measurements at a resolution of 4 cm^{−1} under N₂ or CO₂ gas flow at 1.5 L min^{−1}. For the transmittance mode in case of E-T, a thin sample film was used to ensure that the band absorbance were in the Lambert-Beer law range. The attenuated total reflection mode was performed for CL-Mx, CL-Dx, and CL-T5 using an ATR PRO ONE (JASCO) with an ATR correction program.

Synchrotron SAXS measurements were performed using the BL-15A2 beamline at the Photon Factory of the High Energy Accelerator Research Organization (KEK) in Tsukuba, Japan. The X-ray wavelength was 0.092 nm, and PILATUS 2 M was used as a detector. Stearic acid and silver behenate were used as calibration standards. Samples fully exposed to CO₂ gas were quickly installed into the beamline and measured in air. For in situ SAXS measurements with stretching, a custom-made tensile device (AcroEdge Co., Ltd.) with a sample chamber was installed in the beamline and the specimen was stretched at 0.09 s^{−1}. CO₂ gas was flown into the sample chamber at 3.0 L min^{−1}. Prior to the measurement, the specimen was exposed to CO₂ gas for 1.5 h in the sample chamber.

A rheometer (MCR302, Anton Paar) with 4-mm-diameter plates was used for linear viscoelasticity measurements. A shear strain of 0.1% was applied at 1 Hz. A temperature sweep test was conducted from −30 °C to 150 °C using a Peltier cooling system at a heating rate of 3 °C min^{−1}. A flow rate of 3.0 L min^{−1} was used for each dry gas. DMA measurements were performed using an MCR702e instrument (Anton Paar). Measurements were performed in the tensile mode at 1 Hz with a tensile strain of 0.1% and at constant temperature (25 °C). The sample dimensions were 20 mm × 5.0 mm × 1.0 mm and 20 mm × 5.0 mm × 0.2 mm for CL-D9 and E-T, respectively. Dry N₂ and CO₂ gases were flown into the sample chamber at a rate of 3.0 L min^{−1}.

Tensile and compression measurements were conducted using an AND force tester MCT-2150 with a custom-made sample chamber at 26 °C ± 1 °C. N₂ or CO₂ gases were flown into the chamber at 3.0 L min^{−1}. Sample pieces for tensile tests were shaped into JIS 7 dumbbell-shaped tensile bars. Prior to the measurement, the specimen was exposed to dry N₂ or CO₂ gas for more than 2 h in the sample chamber. The initial gauge length was set to ~20 mm. The sample pieces were stretched at 100 mm min^{−1}. For compression tests, a sample block (5 mm × 5 mm × 5 mm) was compressed at 100 mm min^{−1}. Tearing tests were performed using an AND force tester MCT-2150 at 26 °C ± 1 °C. Trouser-shaped test pieces were torn at 100 mm min^{−1}. Prior to the measurement, the specimen was exposed to dry N₂ or CO₂ gas for more than 2 h in the sample chamber. The fracture energy was calculated following the literature⁴⁰.

Data availability

The authors declare that the data supporting the findings of this study are available within the article and its Supplementary Information files are available from the authors upon reasonable request.

Received: 21 August 2023; Accepted: 9 February 2024;

Published online: 05 March 2024

References

- Morison, J. I. L. & Gifford, R. M. Stomatal sensitivity to carbon dioxide and humidity: a comparison of two C3 and two C4 grass species. *Plant Physiol.* **71**, 789–796 (1983).
- Gillies, M. T. The role of carbon dioxide in host-finding by mosquitoes (Diptera: Culicidae): a review. *Bull. Entomol. Res.* **70**, 525–532 (1980).
- Lin, S. & Theato, P. CO₂-responsive polymers. *Macromol. Rapid Commun.* **34**, 1118–1133 (2013).
- Zhang, Q., Lei, L. & Zhu, S. Gas-responsive polymers. *ACS Macro Lett.* **6**, 515–522 (2017).
- Liu, H., Lin, S., Feng, Y. & Theato, P. CO₂-responsive polymer materials. *Polym. Chem.* **8**, 12–23 (2017).
- Cunningham, M. F. & Jessop, P. G. Carbon dioxide-switchable polymers: where are the future opportunities? *Macromolecules* **52**, 6801–6816 (2019).
- Carretti, E., Dei, L., Baglioni, P. & Weiss, R. G. Synthesis and characterization of gels from polyallylamine and carbon dioxide as gellant. *J. Am. Chem. Soc.* **125**, 5121–5129 (2003).
- Endo, T., Nagai, D., Monma, T., Yamaguchi, H. & Ochiai, B. A novel construction of a reversible fixation–release system of carbon dioxide by amidines and their polymers. *Macromolecules* **37**, 2007–2009 (2004).
- Nagai, D., Suzuki, A., Maki, Y. & Takeno, H. Reversible chain association/dissociation via a CO₂ responsive crosslinking/decrosslinking system. *Chem. Commun.* **47**, 8856–8858 (2011).
- Yan, Q. et al. CO₂-responsive polymeric vesicles that breathe. *Angew. Chem. Int. Ed.* **50**, 4923–4927 (2011).
- Lei, L., Zhang, Q., Shi, S. & Zhu, S. Oxygen and carbon dioxide dual gas-responsive and switchable microgels prepared from emulsion copolymerization of fluoro- and amino-containing monomers. *Langmuir* **31**, 2196–2201 (2015).
- Chen, L., Liu, R. & Yan, Q. Polymer meets frustrated Lewis pair: second-generation CO₂-responsive nanosystem for sustainable CO₂ conversion. *Angew. Chem.* **130**, 9480–9484 (2018).
- Chen, L., Liu, R., Hao, X. & Yan, O. CO₂-cross-linked frustrated Lewis networks as gas-regulated dynamic covalent materials. *Angew. Chem.* **131**, 270–274 (2019).
- George, M. & Weiss, R. G. Chemically reversible organogels: aliphatic amines as “latent” gelators with carbon dioxide. *J. Am. Chem. Soc.* **123**, 10393–10394 (2001).
- George, M. & Weiss, R. G. Chemically reversible organogels via “latent” gelators. aliphatic amines with carbon dioxide and their ammonium carbamates. *Langmuir* **18**, 7124–7135 (2002).
- Yu, T., Wakuda, K., Blair, D. L. & Weiss, R. G. Reversibly cross-linking amino-polysiloxanes by simple triatomic molecules. Facile methods for tuning thermal, rheological, and adhesive properties. *J. Chem. Phys. C* **113**, 11546–11553 (2009).
- Perry, R. J. & O’Brien, M. J. Amino disiloxanes for CO₂ capture. *Energy Fuels* **25**, 1906–1918 (2011).
- Fischer, V., Landfester, K. & Muñoz-Espí, R. Molecularly controlled coagulation of carboxyl-functionalized nanoparticles prepared by surfactant-free miniemulsion polymerization. *ACS Macro Lett.* **1**, 1371–1374 (2012).
- Jia, Y.-G., Zhang, M. & Zhu, X. X. CO₂-switchable self-healing host–guest hydrogels. *Macromolecules* **50**, 9696–9701 (2017).
- Wang, X. et al. Salt-enhanced CO₂-responsiveness of microgels. *ACS Macro Lett.* **9**, 1611–1616 (2020).
- Rudkevich, D. M. & Xu, H. Carbon dioxide and supramolecular chemistry. *Chem. Commun.* 2651–2659 (2005).
- Liu, R., Wang, Y. & Yan, Q. CO₂-strengthened double-cross-linked polymer gels from frustrated Lewis pair networks. *Macromol. Rapid Commun.* **42**, 2000699 (2021).
- Yang, Y. & Urban, M. W. Self-repairable polyurethane networks by atmospheric carbon dioxide and water. *Angew. Chem. Int. Ed.* **53**, 12142–12147 (2014).
- Miwa, Y., Taira, K., Kurachi, J., Udagawa, T. & Kutsumizu, S. A gas-plastic elastomer that quickly self-heals damage with the aid of CO₂ gas. *Nat. Commun.* **10**, 1828 (2019).

25. Poon, L. & Weiss, R. G. Uncharged Lewis bases yield polydimethylsiloxane ionomers with amidinium alkyldithiocarbamate side chains. *J. Phys. Chem.* **59**, 2345–2354 (2021).
26. Poon, L., Hum, J. R. & Weiss, R. G. Effects of cyclic and acyclic amidine side-chains on the properties of polysiloxane ionomers constructed in situ from three uncharged components. *Soft Matter* **18**, 5502–5508 (2022).
27. Li, A. et al. A novel crack healing in steels by gas nitrocarburizing. *Appl. Surf. Sci.* **442**, 437–445 (2018).
28. Edvardsen, C. Water permeability and autogenous healing of cracks in concrete. *ACI Mater. J.* **96**, 448–454 (1999).
29. Jeon, J. W. et al. Highly carboxylate-functionalized polymers of intrinsic microporosity for CO₂-selective polymer membranes. *Macromolecules* **50**, 8019–8027 (2017).
30. Xu, X. et al. High-efficiency CO₂ separation using hybrid LDH-polymer membranes. *Nat. Commun.* **12**, 3069 (2021).
31. Gargiulo, N., Pepe, F. & Caputo, D. CO₂ adsorption by functionalized nanoporous materials: a review. *J. Nanosci. Nanotechnol.* **14**, 1811–1822 (2014).
32. Koizumi, H. et al. One-pot catalytic synthesis of urea derivatives from alkyl ammonium carbamates using low concentrations of CO₂. *Commun. Chem.* **4**, 66 (2021).
33. Xie, W. et al. Metal-free reduction of CO₂ to formate using a photochemical organohydride-catalyst recycling strategy. *Nat. Chem.* **15**, 794–802 (2023).
34. Yu, Y., Fang, L.-M., Liu, Y. & Lu, X.-B. Chemical synthesis of CO₂-based polymers with enhanced thermal stability and unexpected recyclability from biosourced monomers. *ACS Catal.* **11**, 8349–8357 (2021).
35. Yang, G.-W. et al. Precision copolymerization of CO₂ and epoxides enabled by organoboron catalysts. *Nat. Synth.* **1**, 892–901 (2022).
36. Kuo, A. C. M. *Poly(dimethylsiloxane): Polymer Data Handbook*, Mark, J. E. (ed.) (Oxford University Press, 1999).
37. Yarusso, D. J. & Cooper, S. L. Analysis of SAXS data from ionomer systems. *Polymer* **26**, 371–378 (1985).
38. Kutsumizu, S., Goto, M., Yano, S. & Schlick, S. Structure and dynamics of ionic aggregates in ethylene ionomers and their effect on polymer dynamics: a study of small-angle X-ray scattering and electron spin resonance spectroscopy. *Macromolecules* **35**, 6298–6305 (2002).
39. Mullins, L. Rupture of rubber. IX. Role of hysteresis in the tearing of rubber. *Trans. Inst. Rubber Ind.* **35**, 213–221 (1959).
40. Matsuda, T., Kawakami, R., Nakajima, T., Hane, Y. & Gong, J. P. Revisiting the origins of the fracture energy of tough double-network hydrogels with quantitative mechanochemical characterization of the damage zone. *Macromolecules* **54**, 10331–10339 (2021).
41. Zheng, Y. et al. Nanophase separation in immiscible double network elastomers induces synergetic strengthening, toughening, and fatigue resistance. *Chem. Mater.* **33**, 3321–3334 (2021).
42. Miwa, Y., Ohya, T., Takagi, H. & Kutsumizu, S. In situ SAXS observation of transient network behavior in ionically cross-linked polydimethylsiloxane elastomer with slow and fast stretching. *Macromolecules* **55**, 9126–9133 (2022).
43. Sun, J.-Y. et al. Highly stretchable and tough hydrogels. *Nature* **489**, 133–136 (2012).

Acknowledgements

YM is grateful to Prof. N. A. Lynd (University of Texas, Austin) and Prof. G. E. Sanoja (University of Texas, Austin) for the fruitful discussions. Beam time at PF-KEK provided by Programs 2019G116, 2020G610, and 2021G573 is acknowledged herein. This research was financially supported by the JSPS KAKENHI Grant Numbers 19K05612 (YM) and 22H02141 (YM); JST, PRE-STO Grant Number JPMJPR199B (YM), Japan; CCI Grant Program (YM).

Author contributions

Y. M. planned and directed the project, Y. M., H. Y., T. O., H. N., R. T., K. O., and S. S. conducted the experiments. Y. M., H. Y., T. O., H. N., R. T., K. O., S. S., K. H., and S. K. analyzed and discussed about the data; Y. M., K. H., and S. K. wrote the paper. All authors have given approval to the final version of the manuscript.

Competing interests

The authors declare no competing interests.

Additional information

Supplementary information The online version contains supplementary material available at <https://doi.org/10.1038/s43246-024-00457-9>.

Correspondence and requests for materials should be addressed to Yohei Miwa.

Peer review information *Communications Materials* thanks Izumi Ichinose, Yi Cao and the other, anonymous, reviewer(s) for their contribution to the peer review of this work. Primary Handling Editors: Jet-Sing Lee. A peer review file is available.

Reprints and permissions information is available at <http://www.nature.com/reprints>

Publisher's note Springer Nature remains neutral with regard to jurisdictional claims in published maps and institutional affiliations.

Open Access This article is licensed under a Creative Commons Attribution 4.0 International License, which permits use, sharing, adaptation, distribution and reproduction in any medium or format, as long as you give appropriate credit to the original author(s) and the source, provide a link to the Creative Commons licence, and indicate if changes were made. The images or other third party material in this article are included in the article's Creative Commons licence, unless indicated otherwise in a credit line to the material. If material is not included in the article's Creative Commons licence and your intended use is not permitted by statutory regulation or exceeds the permitted use, you will need to obtain permission directly from the copyright holder. To view a copy of this licence, visit <http://creativecommons.org/licenses/by/4.0/>.

© The Author(s) 2024